An Insight into the Process Involved in Hydrothermal Conversion of FAU to *BEA Zeolite

Hery Jon, Nobuaki Ikawa, Yasunori Oumi, and Tsuneji Sano*

Department of Applied Chemistry, Graduate School of Engineering, Hiroshima University, Higashi-Hiroshima 739-8527, Japan

Received December 24, 2007. Revised Manuscript Received February 26, 2008

The use of FAU zeolite as a starting material was found to enhance the crystallization rate of *BEA zeolite, suggesting that the dissolution of FAU zeolite provides locally ordered aluminosilicate species that assemble and evolve into *BEA zeolite. Here we show experimental findings that indicate the presence of such locally ordered aluminosilicate species in intermediate phases involved in the hydrothermal conversion of FAU zeolite into *BEA zeolite. On the basis of the previous fact that cetyltrimethylammonium (CTA^+) cations seem to be able to preserve zeolitic fragments or seeds and retain them in the mesoporous framework, this method was applied to the characterization of the obtained intermediate phases. From the detailed characterization of mesoporous products, the different characteristics were found to be observed between intermediate phases. Namely, as the more disordered arrangement was found in the mesoporous products, the presence of evolved, locally ordered aluminosilicate species was strongly indicated.

Introduction

As summarized by Cundy et al.,[1] several crystallization mechanisms concerning the hydrothermal synthesis of zeolites have been proposed during the last six decades; however, the crystallization process has not been fully understood. Accordingly, the crystallization mechanism study still attracts zeolite researchers.[2,3] Recently, our group has focused on zeolite synthesis by the hydrothermal conversion of one zeolite into another, i.e. interzeolite transformation. In the hydrothermal conversion of FAU zeolite into *BEA zeolite, it was found that when a small amount of tetraethylammonium hydroxide (TEAOH) was added as an alkali source, the use of FAU zeolite as starting material showed the enhanced crystallization rate of *BEA zeolite as compared to amorphous silica/γ-alumina.[4] Moreover, in tetramethylammonium hydroxide (TMAOH) media, the FAU zeolite was converted into highly crystalline RUT zeolite faster than the amorphous silica/γ-alumina.[5] These phenomena led us to the hypothesis that the dissolution of FAU zeolite under a specific SDA (structure-directing agent) provides locally ordered aluminosilicate species that readily build up a particular zeolite framework, indicating that an interzeolite transformation synthesis route affords an attractive study.

Since the work of scientists at Mobil Oil Research and Development in 1992,[6] there has been a lot of research concerning the synthesis of supramolecular-templated mesoporous materials. In the very short period of time since its invention, a large number of potential applications of these materials have been developed in the area of catalysis, separation, and advanced materials.[7,8] In order to be used as a solid-acid catalyst in comparison to crystalline microporous zeolites, however, mesoporous aluminosilicates lack hydrothermal stability and strong acidity due to their noncrystalline framework walls. Thus, several attempts to synthesize mesoporous aluminosilicates with crystalline walls have been reported.[9] The significant progress toward the zeolitization of mesoporous aluminosilicates was pioneered by the van Bekkum group via partially recrystallizing mesoporous framework walls into nanosized ZSM-5 zeolite.[10] Then, Pinnavaia et al. established a novel route involving a direct assembly of FAU zeolite seeds,[11] as well as MFI and *BEA zeolites seeds[12] in cetyltrimethylammonium bromide (CTAB) media into steam-stable mesoporous aluminosilicates. Almost coincidentally, Xiao et al. proposed

* Corresponding author. E-mail: tsano@hiroshima-u.ac.jp. Phone: +81-82-424-7607. Fax: +81-82-424-5494.

(1) Cundy, C. S.; Cox, P. A. *Microporous Mesoporous Mater.* **2005**, *82*, 1.
(2) Davis, T. M.; Drews, T. O.; Ramanan, H.; He, C.; Dong, J.; Schnablegger, H.; Katsoulakis, M. A.; Kokkoli, E.; McCormick, A. V.; Penn, R. L.; Tsapatsis, M. *Nat. Mater.* **2006**, *5*, 400.
(3) Kubota, Y.; Maekawa, H.; Miyata, S.; Tatsumi, T.; Sugi, Y. *Microporous Mesoporous Mater.* **2007**, *101*, 115.
(4) Jon, H.; Nakahata, K.; Lu, B. W.; Oumi, Y.; Sano, T. *Microporous Mesoporous Mater.* **2006**, *96*, 72.
(5) Jon, H.; Takahashi, S.; Sasaki, H.; Oumi, Y.; Sano, T. *Microporous Mesoporous Mater.*, in press.
(6) Kresge, C. T.; Leonowicz, M. E.; Roth, W. J.; Vartuli, J. C.; Beck, J. S. *Nature* **1992**, *359*, 710. (a) Beck, J. S.; Vartuli, J. C.; Roth, W. J.; Leonowicz, M. E.; Kresge, C. T.; Schmitt, K. D.; Chu, C. T-W.; Olson, D. H.; Sheppard, E. W.; McCullen, S. B.; Higgins, J. B.; Schlenker, J. L. *J. Am. Chem. Soc.* **1992**, *114*, 10834.
(7) Sayari, A. *Chem. Mater.* **1996**, *8*, 1840.
(8) Vartuli, J. C.; Degnan, T. F. Introduction to Zeolite Science and Practice. In *Studies in Surface Science and Catalysis*, 3rd ed.; Èjka, J., van Bekkum, H., Corma, A., Schüth, F., Eds.; Elsevier, 2007, *168*, 837.
(9) Liu, Y.; Pinnavaia, T. J. *J. Mater. Chem.* **2002**, *12*, 3179.
(10) Kloetstra, K. R.; van Bekkum, H.; Jansen, J. C. *Chem. Commun.* **1997**, 2281.
(11) Liu, Y.; Zhang, W.; Pinnavaia, T. J. *J. Am. Chem. Soc.* **2000**, *122*, 8791.
(12) Liu, Y.; Zhang, W.; Pinnavaia, T. J. *Angew. Chem., Int. Ed.* **2001**, *40*, 1255.

10.1021/cm703676y CCC: $40.75
Published on Web 05/23/2008

a synthesis of mesoporous aluminosilicates with ordered hexagonal structure, strong acidity, and extraordinary hydrothermal stability at high temperatures made from *BEA zeolite precursor.[13] By using filtrate of an alkaline dissolution of ZSM-5 zeolite, Matsukata group synthesized MCM-41-type mesoporous materials containing ZSM-5 zeolite fragments.[14] Very recently, via a hydrothermal treatment of CTA-intercalated, layered silicate Na-RUB-18, Pérez-Pariente and co-workers have succeeded in the synthesis of mesoporous materials retaining plate-like morphology and most of the local ordering of the parent material.[15] Moreover, the Pinnavaia group has revealed that the zeolitic subunits could be stabilized through the base hydrolysis of ZSM-5 in the presence of CTA^+ cations.[16] The above facts strongly suggest that CTA^+ cations have a functionality to stabilize zeolitic precursors, seeds and/or fragments besides the main functionality as a supermolecular template.

From such viewpoints, it seems to be possible to preserve locally ordered aluminosilicate species present during the hydrothermal conversion of zeolite in mesoporous materials prepared with CTA^+ cations. By thoroughly investigating the properties of mesoporous products, there must be useful information that may lead us to understand the mechanism of hydrothermal conversion of zeolite. Here we report the formation of mesoporous aluminosilicates in CTAB media from intermediate phases involved in the hydrothermal conversion of FAU zeolite into *BEA zeolite as well as the detailed characteristics of the mesoporous products.

Experimental Section

Synthesis. The hydrothermal conversion procedure was described in detail in our previous paper.[4] Typically, dealuminated FAU zeolite with a Si/Al ratio of 23 was mixed well with an aqueous solution of tetraethylammonium hydroxide. The starting molar ratio was set to $SiO_2/0.0215Al_2O_3/0.2TEAOH/5H_2O$. Then, the mixture was transferred into a 30-cm^3 Teflon-lined stainless steel autoclave and was statically heated at 140 °C for 2−144 h in a convection oven. After being heated for a prescribed time, the autoclave was cooled down and then the solid phase was thoroughly mixed with an aqueous solution of cetyltrimethylammonium bromide (CTAB) for 30 min using a magnetic stirrer. To homogenously dissolve CTAB, the mixture of CTAB and water was heated at 60 °C for 10 min and stirred until clear solution was obtained. The total molar ratio of the gel was $SiO_2/0.0215Al_2O_3/0.2TEAOH/0.15CTAB/40H_2O$. Then, the mixture was heated again at 150 °C for 5 days in the convection oven. The mesoporous products were filtered and washed with warm water (60 °C) and dried at 70 °C overnight. The calcination was conducted at 500 °C for 10 h to remove the organic compounds: TEAOH and CTAB. The as-made and calcined samples were referred to as M*x* h and calM*x* h, respectively, where *x* denoted the crystallization time before adding CTAB.

Characterization. The X-ray diffraction (XRD) patterns of the solid products were collected using a powder X-ray diffractometer (Bruker AXS D8 Advance) with graphite monochromatized Cu Kα radiation at 40 kV and 30 mA. The crystal morphology was observed by scanning electron microscopy (SEM, JEOL JSM-6320FS). Transmission electron microscopy (TEM) images were taken using a JEOL JEM-2010 microscope. Nitrogen adsorption isotherms at −196 °C were performed using a conventional volumetric apparatus (Bel Japan, BELSORP 28SA). Prior to adsorption measurements, the calcined samples (0.1 g) were evacuated at 400 °C for 10 h. The IR spectra were recorded on a FTIR spectrometer (JEOL JIR-7000) with a resolution of 4 cm^{-1} at room temperature. For OH group stretching region measurements, the sample was pressed into a self-supporting thin wafer (6.4 mg cm^{-2}) and placed into a quartz IR cell equipped with CaF_2 windows. Prior to measurement, each sample was dehydrated under vacuum at 400 °C for 2 h. For acidity measurements, self-supporting thin wafer samples were degassed at 400 °C for 2 h under vacuum and subsequently recorded at RT as background spectra. Then pyridine was admitted at RT for 1 h to reach adsorption equilibrium and degassed at 250 °C for 1 h. Next, the spectra were recorded at RT and the background subtracted. For the KBr method, 1 wt% of sample was mixed well with KBr and pressed into a thin wafer. Prior to measurement at RT, the thin wafer was dehydrated at 200 °C for 2 h in the quartz IR cell equipped with KBr windows. ^{27}Al MAS NMR spectra were recorded using a 7-mm diameter zirconia rotor on a Bruker DRX-400 spectrometer at 104.2 MHz. The rotor was spun with dry air at 4 kHz. The spectra were accumulated with 1.0-μs pulses, 1-s recycle delay, and 4000 scans. $Al(NO_3)_3 \cdot 9H_2O$ was used as a chemical shift reference. Prior to ^{27}Al MAS NMR measurements, the samples were moisture-equilibrated over a saturated solution of NH_4Cl for 24 h. ^{29}Si MAS NMR spectra were also recorded on the same spectrometer at 79.5 MHz with a spinning rate of 4 kHz, 10-μs pulses, 1-s recycle delay, and 4000 scans. $Si(CH_3)_4$ was used as a chemical shift reference.

Catalytic Test. Cumene cracking activity was used to evaluate the acidity of the obtained mesoporous products. The reaction was carried out in an atmospheric pressure flow system. The catalyst, placed into a 10-mm inner diameter quartz tube reactor, was dehydrated at 400 °C for 1 h under nitrogen gas flow. The temperature was then brought down to a reaction temperature of 300 °C. The reactant was fed into the catalyst bed with a microfeeder. Nitrogen gas was used as a carrier gas with flow rate of 40 mL min^{-1}. The contact time (W/F) was 1.88 g h mol^{-1}, and the partial pressure of cumene was 7.9 kPa. An online product analysis was performed by a Shimadzu GC-17A gas chromatograph (equipped with a FID detector) with a GL-Science TC-1 capillary column (30 m). The commercial *BEA zeolite from Tosoh Co., Ltd. with almost a similar Si/Al ratio (Si/Al = 21) was subjected to the test for comparison.

Results and Discussion

Identification of Intermediate Phases. As shown in Figure 1, after heating for 2 h, the typical peaks corresponding to FAU zeolite remarkably disappeared and then the peaks corresponding to *BEA zeolite (i.e., a sharp peak at $2\theta \approx 22.4°$ and a broad peak at $2\theta \approx 7.5°$) were initially observed after 24 h of heating. It is presumed that during 24 h of heating, the FAU zeolite decomposed and the nucleation of *BEA zeolite occurred. To follow the changes in microscopic scale of such a system during the conversion, the intermediate phases were subjected to several analyses. It is well-known that FTIR spectroscopy is one useful technique to observe the lattice vibrations of zeolites based on the vibration frequencies in the range between 200 and

(13) Zhang, Z. T.; Han, Y.; Zhu, L.; Wang, R. W.; Yu, Y.; Qiu, S. L.; Zhao, D. Y.; Xiao, F. S. *Angew. Chem., Int. Ed.* **2001**, *40*, 1258. Zhang, Z. T.; Han, Y.; Xiao, F. S.; Qiu, S. L.; Zhu, L.; Wang, R. W.; Yu, Y.; Zhang, Z.; Zou, B. S.; Wang, Y. Q.; Sun, H. P.; Zhao, D. Y.; Wei, Y. *J. Am. Chem. Soc.* **2001**, *123*, 5014.
(14) Inagaki, S.; Ogura, M.; Inami, T.; Sasaki, Y.; Kikuchi, E.; Matsukata, M. *Microporous Mesoporous Mater.* **2004**, *74*, 163.
(15) García, R.; Díaz, I.; Márquez-Álvarez, C.; Pérez-Pariente, J. *Chem. Mater.* **2006**, *18*, 2283.
(16) Wang, H.; Liu, Y.; Pinnavaia, T. J. *J. Phys. Chem. B* **2006**, *110*, 4524.

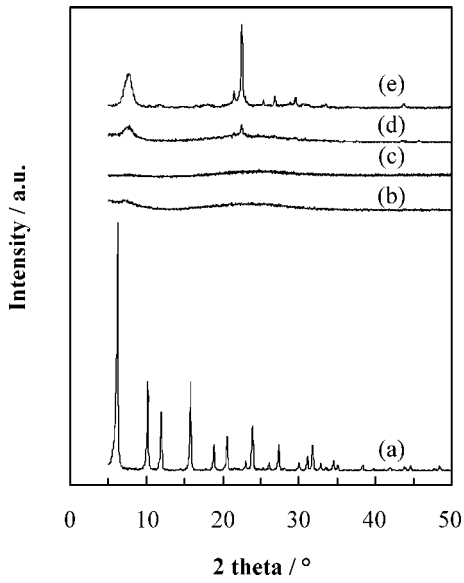

Figure 1. XRD patterns of as-made solid products obtained at different crystallization times during hydrothermal conversion of FAU zeolite into *BEA zeolite: (a) 0 h, (b) 2 h, (c) 18 h, (d) 24 h, and (e) 144 h.

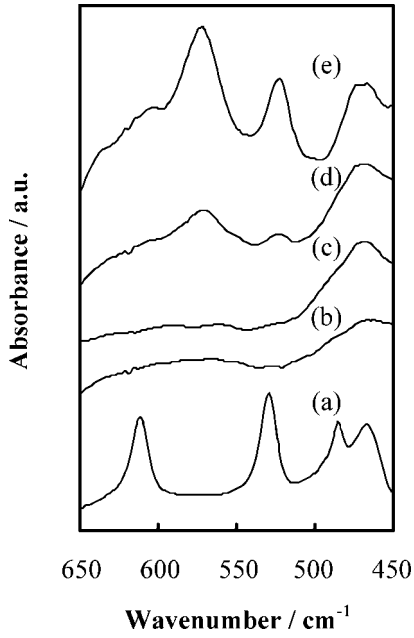

Figure 2. FTIR spectra in the rings vibration region of as-made solid products obtained at different crystallization times during hydrothermal conversion of FAU zeolite into *BEA zeolite: (a) 0 h, (b) 2 h, (c) 18 h, (d) 24 h and (e) 144 h.

1500 cm^{-1}.[17–20] Figure 2 shows the FTIR spectra of ring vibrations for phases involved in the conversion process. As can be seen in Figure 2a, the 0 h heated sample exhibited typical ring vibrations of a FAU zeolite. The well-identified four sharp peaks at 468, 485, 530, and 613 cm^{-1} were observed. Peaks at 468 and 485 cm^{-1} were attributed to internal T−O−T bending vibration; whereas peaks at 530 and 613 cm^{-1} were assigned to external T−O−T bending vibration and double six-membered ring (D6R) vibration,

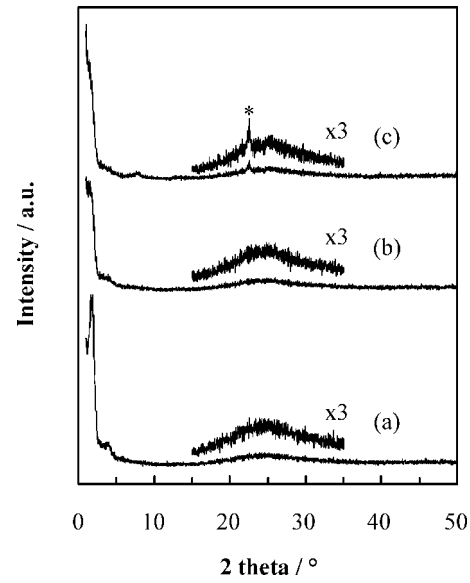

Figure 3. XRD patterns of calcined mesoporous products prepared from intermediate phases obtained at different crystallization times: (a) 2 h, (b) 18 h, and (c) 24 h. The asterisk denotes the typical peak of *BEA zeolite.

respectively.[21] After 2 and 18 h of heating, the peaks corresponding to the FAU zeolite framework vibrations disappeared and only broad peaks were observed (Figure 2, parts b and c). Figure 2d shows the spectrum of the 24 h heated sample. Four distinct peaks could be identified. The peak at 474 cm^{-1} was assigned to internal T−O−T bending vibration; whereas the peak at 525 cm^{-1} was external T−O−T bending vibration (see above). The intensity of the peak at 525 cm^{-1} became higher, indicating that more crystalline *BEA zeolite crystals evolved after 24 h of heating. The peak at 575 was attributed to 5R vibration.[20] The spectrum of highly crystalline *BEA zeolites (Figure 2e) exhibited more intense peaks as compared to those in Figure 2d, indicating a more ordered microscopic arrangement. However, the data required for deducing the conclusion regarding the conversion process of FAU zeolite into *BEA zeolites are still inadequate. As described in the Introduction, in the presence of CTA^+ cations, it is possible to preserve zeolitic precursors, seeds, and/or fragments via the formation of mesoporous materials; we apply this method to the intermediate phases and characterize the obtained mesoporous materials in detail.

Characterization of Mesoporous Materials. The preparation of mesoporous materials from intermediate phases present during the hydrothermal conversion of FAU zeolite into *BEA zeolite was carried out by adding CTAB solution into the gel mixture obtained at different crystallization times, followed by subsequent hydrothermal treatment at 150 °C for 5 days. Figure 3 shows the XRD patterns of the calcined mesoporous products. It is clear that increasing the crystallization time from 2 to 18 h rendered the peak at low angle less intense, indicating that the mesoporous parts remarkably decreased (Figures 3, parts a and b). Moreover, in the XRD pattern of the mesoporous product from the intermediate

(17) Flanigen, E. M.; Khatami, H.; Szymanski, H. A. *ACS Ser.* **1971**, *101*, 201.
(18) Blackwell, C. S. *J. Phys. Chem.* **1979**, *83*, 3251.
(19) Blackwell, C. S. *J. Phys. Chem.* **1979**, *83*, 3257.
(20) Mozgawa, W. *J. Mol. Struct.* **2001**, *596*, 129.
(21) Halasz, I.; Agarwal, M.; Marcus, B.; Cormier, W. E. *Microporous Mesoporous Mater.* **2005**, *84*, 318.

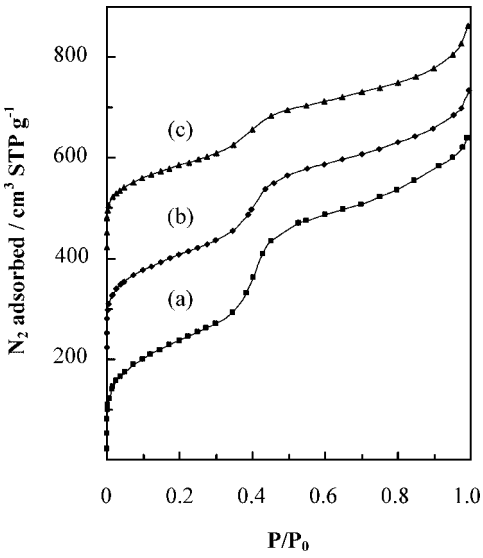

Figure 4. Nitrogen adsorption isotherms of calcined mesoporous products prepared from intermediate phases obtained at different crystallization times: (a) 2 h, (b) 18 h, and (c) 24 h. The isotherms are offset by 200 cm^3 (STP) g^{-1}.

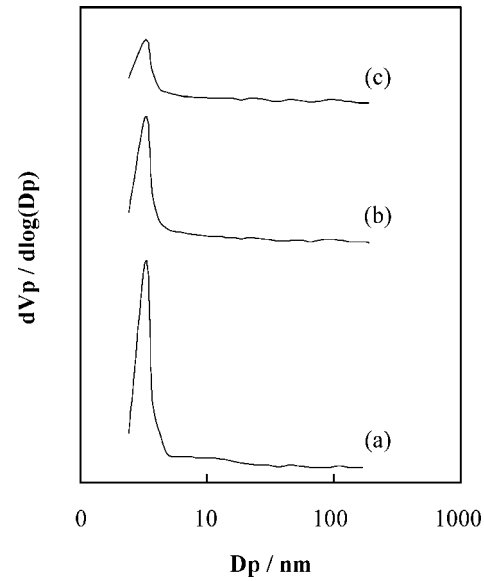

Figure 5. BJH pore size distribution curves (derived from adsorption branch) for calcined mesoporous products prepared from intermediate phases obtained at different crystallization times: (a) 2 h, (b) 18 h, and (c) 24 h.

phase after 24 h of heating, where the peak of *BEA zeolite was observed, the peak at low angle almost disappeared (Figure 3c). Although it was difficult to identify the differences between phases during the hydrothermal conversion of zeolite, this method demonstrated that the differences between them are more noticeable. Furthermore, as compared to MCM-41 with ordered hexagonal-arranged channels and consequently with sharp peaks attributed to hexagonal structure, the XRD pattern of sample calM2 h is likely similar to disordered mesoporous material.[22]

Figure 4 shows nitrogen adsorption isotherms of the corresponding mesoporous products. All of the isotherms demonstrated the type IV isotherm, that is, the characteristic isotherm of mesoporous materials. The inflection point was observed at a relative pressure $p/p_0 \approx 0.4$. This corresponds to the filling of mesopores and the sharp increase in the adsorbed volume indicates a uniform pore size distribution. It became apparent that with increasing crystallization time, the increase in the adsorbed volume seems to decline. It means that the number of mesoporous channels decreased from 2 to 24 h of heating and finally disappeared for 30 h of heating (not shown). In addition, BJH pore size distribution curves of the mesoporous products are exhibited in Figure 5. All of the samples possess a narrow pore size distribution centered at 3.3 nm. The textural properties of the obtained mesoporous products are listed in Table 1. It is noticeable that all of the mesoporous products possess high specific surface area and high total pore volume, that are characteristics of mesoporous materials. However, with the increase in the crystallization time, the specific surface area and the total pore volume remarkably decreased.

Electron microscopy techniques were used to study the morphology and pore arrangements of the obtained mesoporous products. Figure 6 shows the TEM and SEM images of samples M2 h and M18 h. The TEM images clearly showed that both samples have wormhole-like pore arrangements (Figure 6, parts A1 and A2). These TEM observation results confirm the previous XRD results, that the obtained mesoporous products consisted of channels with disordered arrangements. Furthermore, the SEM images of both samples showed the morphology of separated sphere-like particles with 200−500 nm in size along with their agglomerations (Figures 6, parts B1 and B2). As the possibility of physical mixture may be considered in these systems, we also performed thorough observations using TEM and SEM. However, we did not find any isolated crystalline phases coexisting with the mesoporous materials.

Table 1. Textural Properties of Calcined Mesoporous Products

sample code	d (nm)	APD[a] (nm)	S_{BET}[b] (m^2 g^{-1})	total pore volume[c] (cm^3 g^{-1})
calM2 h	5.16	3.28	855	0.988
calM18 h	5.90	3.28	744	0.812
calM24 h		3.28	655	0.706

[a] APD: average pore diameter (determined using BJH method from adsorption branch). [b] BET specific surface area. [c] Total pore volume at $p/p_0 = 0.99$.

To clarify the chemical states of silicon and aluminum species that constructed the mesoporous frameworks, ^{29}Si and ^{27}Al MAS NMR measurements were performed. Figure 7 shows ^{29}Si MAS NMR spectra of the mesoporous products. Three resonances at around −92, −102, and −112 ppm were observed. They were attributed to Q^2 ($Si(OSi)_2(OH)_2$), Q^3 ($Si(OSi)_3(OH)_1$), and/or $Q^4(1Al)$ ($Si(OSi)_3(OAl)_1$) and Q^4-(0Al) ($Si(OSi)_4$), respectively.[23] As these materials consist of aluminum species, the resonance at around −102 ppm might correspond to both Q^3 and $Q^4(1Al)$. It was found that the intensity of $Q^4(0A1)$ increased with increasing crystallization time from 2 to 18 h (Figures 7, parts a and b), indicating the subsequent polymerization of the silicate

(22) Zhao, D. Y.; Wan, Y. Introduction to Zeolite Science and Practice. In *Studies in Surface Science and Catalysis*, 3rd ed.; Èjka, J., van Bekkum, H., Corma, A., Schüth, F., Eds.; Elsevier, 2007, *168*, 279.

(23) Engelhard, G.; Michel, D. *High-Resolution Solid-State NMR of Silicates and Zeolites*, John Wiley & Sons Inc., 1988.

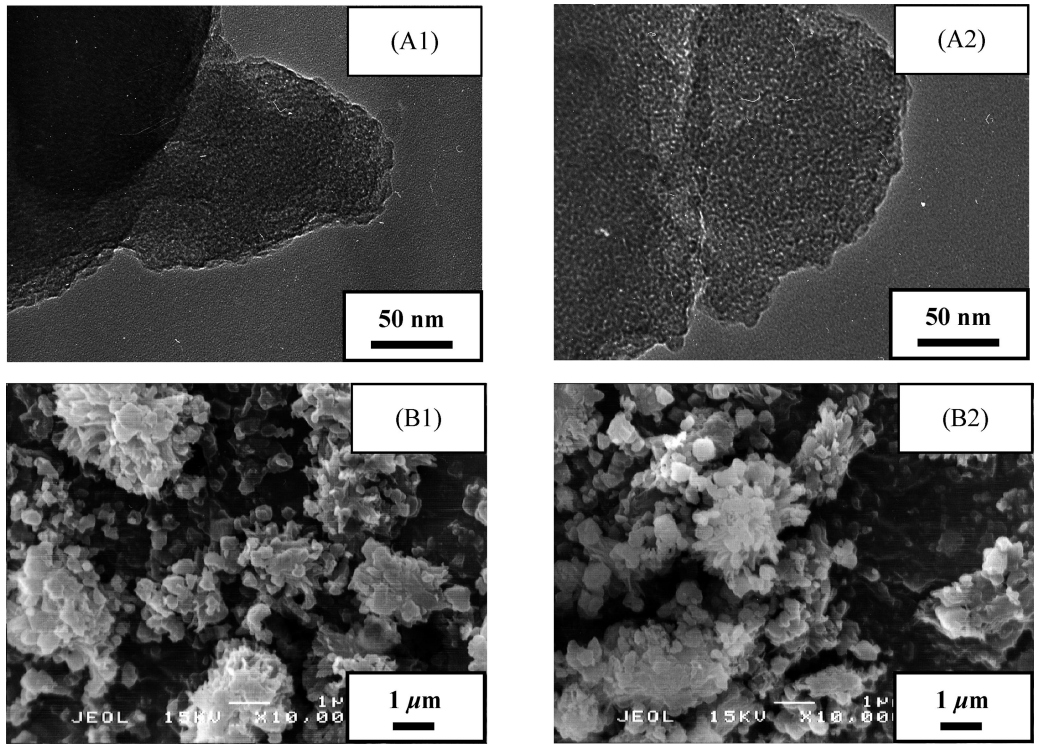

Figure 6. TEM (top, A) and SEM (below, B) images of as-made mesoporous products prepared from intermediate phases obtained at different crystallization times: (1) 2 h and (2) 18 h.

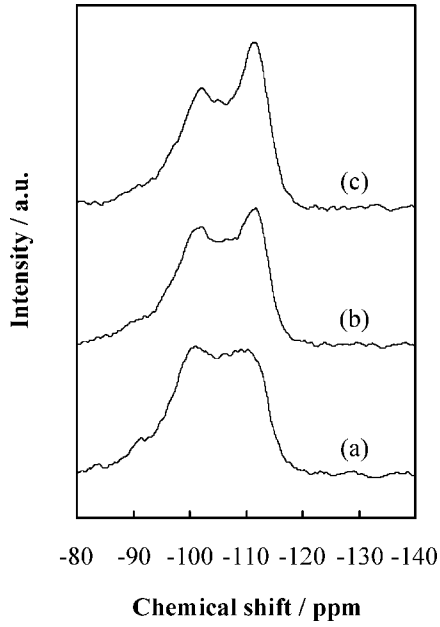

Figure 7. ^{29}Si MAS NMR spectra of as-made mesoporous products prepared from intermediate phases obtained at different crystallization times: (a) 2 h, (b) 18 h, and (c) 24 h.

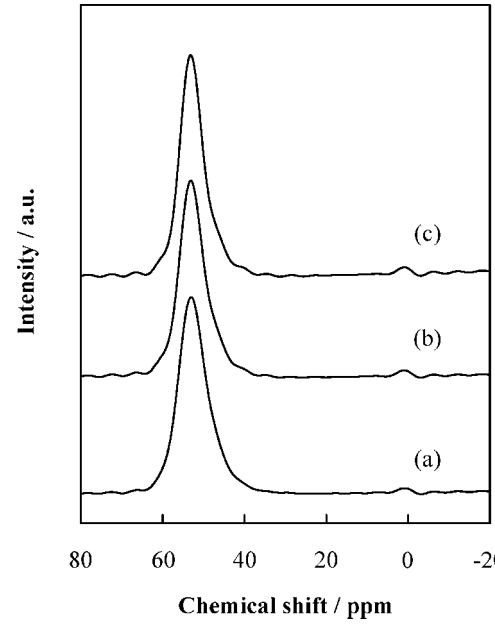

Figure 8. ^{27}Al MAS NMR spectra of as-made mesoporous products prepared from intermediate phases obtained at different crystallization times: (a) 2 h, (b) 18 h, and (c) 24 h.

species. This affords information about the presence of locally more ordered aluminosilicate species within the mesoporous product from the intermediate phase after 18 h of heating. Again, Figure 8 exhibits ^{27}Al MAS NMR spectra of as-made mesoporous products. All samples showed spectra with sharp resonances centered at around 53 ppm, indicating four-coordinated aluminum species (Figure 8A(a)−(c)). It should be noted that fwhm of resonances at around 53 ppm apparently became slightly narrower with increasing crystallization time of intermediate phases. However, after the calcination, all samples underwent a significant decrease in resonance intensity at around 53 ppm, along with increasing intensity of resonances at around 0 ppm, implying severe dealumination (Supporting Information, Figure S1).

The hydroxyl group behavior of mesoporous products was studied based on the FTIR spectra of OH groups stretching vibration region (Figure 9). In sample calM2 h (Figure 9 A(a)), three types of OH groups absorption band were observed at 3780, 3747, and 3680 cm^{-1}, which were assigned to very high frequency absorption (VHF) of terminal

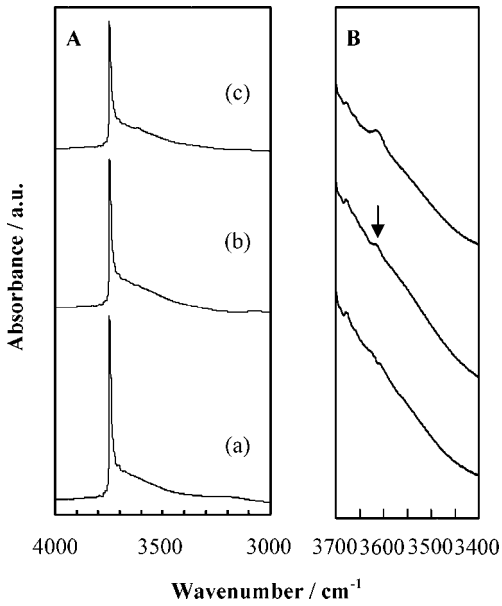

Figure 9. FTIR spectra in the OH stretching region (A) and their magnifications (B) for calcined mesoporous products prepared from intermediate phases obtained at crystallization times: (a) 2 h, (b) 18 h, and (c) 24 h.

hydroxyl groups bonded to nonframework species of AlOOH, isolated terminal silanol groups and hydroxyl groups of aluminum species where the Al atom is connected to the zeolite framework only by one or two remaining chemical bonds, respectively.[24] The band at about 3610 cm^{-1}, attributed to acidic bridging OH groups of Si(OH)Al, was remarkably observed for sample calM24 h, where *BEA zeolite peak was observed by XRD (see the magnification spectra of Figure 9B(c)). Surprisingly, in the case of the sample calM18 h, in which no *BEA zeolite peak was observed by XRD, the weak band attributed to acidic bridging OH groups of Si(OH)Al was also observed. To our knowledge, the evidence for the presence of acidic bridging OH groups of Si(OH)Al within mesoporous aluminosilicates has not been reported elsewhere. For instance, Bein et al. reported the presence of acidic bridging OH groups in micro/meso composite, but not in mesoporous materials.[25] Moreover, after pyridine adsorption, the band at 3610 cm^{-1} completely disappeared (Supporting Information, Figure S2); indicating that strong acidic bridging OH groups are present in the intermediate phase after 18 h of heating and then interact with pyridine molecules. The presence of acidic bridging OH groups indirectly provides adequate information for the presence of locally ordered aluminosilicate species, which was sufficient to develop zeolitic Brönsted acid sites in the amorphous intermediate phase obtained after 18 h of heating.

According to the ^{27}Al MAS NMR results, the calcined mesoporous products possessed commensurate framework aluminum species to generate acidic sites. Therefore, to analyze their acidic properties, an FTIR-monitored pyridine adsorption method was used. The results are shown in Figure 10. As confirmed by the adsorption band of pyridinium cations on Brönsted acid sites (1545 cm^{-1}) and pyridine molecules on Lewis acid sites (1455 cm^{-1}), both mesoporous products generated Brönsted acid sites and Lewis acid sites. The number of acid sites was calculated by using integrated molar extinction coefficients stated by Emeis,[26] i.e., 1.67 cm/μmol for Brönsted acid sites and 2.22 cm/μmol for Lewis acid sites. The B/L ratio of calM2 h and calM18 h were 0.20 and 0.24, respectively. It is clear that calM18 h possessed more Brönsted acid sites than calM2 h, suggesting that more ordered aluminosilicate species were present in calM18 h. This evidence seems to support the results showed by FTIR spectra of OH groups region.

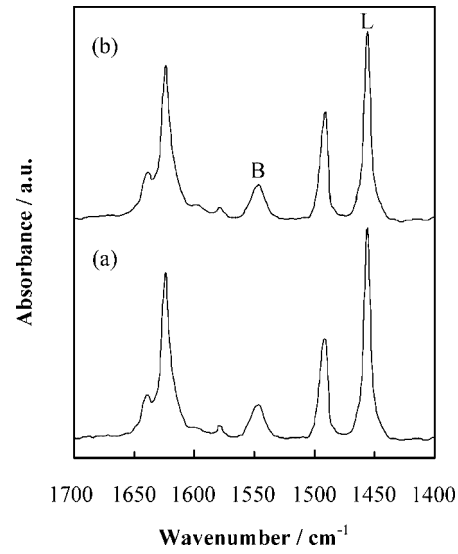

Figure 10. FTIR spectra of pyridine adsorbed at RT for 1 h over calcined mesoporous products prepared from intermediate phases obtained at different crystallization times: (a) 2 h and (b) 18 h. B and L denote Brönsted acid sites and Lewis acid sites, respectively.

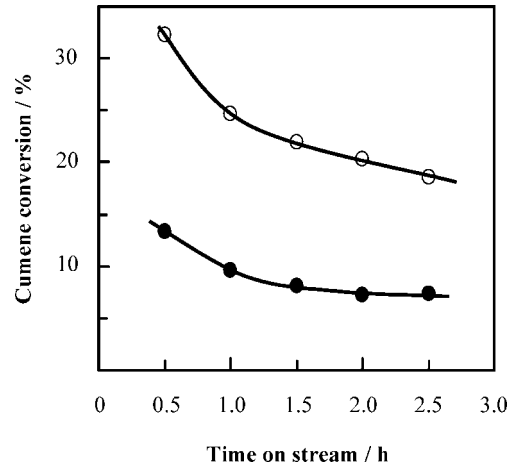

Figure 11. Cumene conversion over (●) calcined M18 h (calM18 h) and (○) commercial *BEA zeolite as a function of time on stream.

From the fact that sample calM18 h showed the presence of zeolitic Brönsted acid sites in the framework, the catalytic activity for cumene cracking was evaluated. Figure 11 shows the cumene conversion over sample calM18 h as a function of time on stream in comparison with a commercial *BEA

(24) Kiricsi, I.; Flego, C.; Pazzuconi, G.; Parker, W. O.; Millini, R.; Perego, C.; Bellussi, G. *J. Phys. Chem.* **1994**, *98*, 4627.
(25) Prokešová, P.; Petkov, N.; Cejka, J.; Mintova, S.; Bein, T. *Collect. Czech. Chem. Commun.* **2005**, *70*, 1829.
(26) Emeis, C. A. *J. Catal.* **1993**, *141*, 347.

zeolite. It was found that the catalytic activity of calM18 h for cumene cracking was almost half of that of the commercial *BEA zeolite. The low activity seems to be due to the difference of four-coordinated aluminum species, as confirmed by ^{27}Al MAS NMR spectra.

We also compared the mesoporous materials from the intermediate phases prepared from amorphous silica/γ-alumina with those from the FAU zeolite. The intermediate phases from amorphous silica/γ-alumina obtained after both 2 and 18 h of heating yielded mesoporous materials with more arranged channels as confirmed by XRD patterns (Supporting Information, Figure S3). The mesoporous products from both FAU zeolite and amorphous silica/γ-alumina were tested for their thermal stability in boiling water. The results indicated that the mesoporous products from FAU zeolite experienced more severe collapse in structure as compared to those from the amorphous silica/γ-alumina. This implies that the more arranged channels show the more stable structure.

All of the above results reveal that during the hydrothermal conversion of FAU zeolite into *BEA zeolite in TEAOH media, the FAU zeolite crystals underwent decomposition into a small and locally ordered aluminosilicate species. These species are then considered to be responsible for the nucleation of *BEA zeolite. However, it should be noted that the detailed structure of locally ordered aluminosilicate species such as nanoslabs[27] cannot be proven. In the presence of CTAB, these species are stabilized and assembled into a mesostructured arrangement. Because the size of locally ordered aluminosilicate is too big to be arranged into an ordered hexagonal arrangement, the packing of channel evolves to disordered arrangement (i.e., a wormhole framework). Consequently, the smaller species yield the more arranged hexagonal structure.

Conclusions

As the enhanced crystallization rate of *BEA zeolite was observed during the hydrothermal conversion of FAU zeolite into *BEA zeolite, we presumed that the dissolution of FAU zeolite provides locally ordered aluminosilicate species that assemble and evolve into *BEA zeolite. By the formation of mesoporous materials in the presence of CTAB, as well as the characterization of mesoporous products, the different characteristics between intermediate phases involved in the hydrothermal conversion of FAU zeolite into *BEA zeolite were observed. According to the XRD patterns, with increasing crystallization time, the arrangement of channels in the mesoporous products became more disordered. The disordered arrangements were also confirmed by TEM images. The nitrogen adsorption test showed that the BET specific surface area, the total pore volume, and the amount of channels with pore diameter of 3.3 nm decreased with increasing crystallization time. ^{29}Si MAS NMR spectra confirmed that there was a significant increase in the intensity of Q^4(0Al) as the crystallization time increased from 2 to 18 h. As confirmed by ^{27}Al MAS NMR spectra, the fwhm of resonances at around 53 ppm assigned to four-coordinated aluminum species became slightly narrower with the increase in crystallization time. Furthermore, the FTIR spectra of the OH group region showed that sample calM18 h possessed a remarkable zeolitic bridging hydroxyl (Si(OH)Al) signal, even the XRD pattern still indicated amorphous structure. The pyridine adsorption spectra also revealed that increasing crystallization time gave rise to increasing the ratio of B/L sites. Compared with the mesoporous material from amorphous silica/γ-alumina prepared at similar crystallization times (2 h), which shows slightly more ordered arrangement, the disordered arrangement of mesoporous material from intermediate phase FAU → *BEA zeolite is likely due to the presence of bigger, locally ordered aluminosilicate species that cannot be arranged into ordered hexagonal arrangement. However, the detailed structure of the species cannot be noticed. In brief, the presence of such locally ordered aluminosilicate species in the intermediate phases involved in the hydrothermal conversion of FAU zeolite into *BEA zeolite may contribute to the enhanced crystallization rate of *BEA zeolite.

Acknowledgment. The authors gratefully acknowledge Prof. S. S. Achmadi from the Department of Chemistry, Bogor Agricultural University for helpful discussions.

Supporting Information Available: ^{27}Al MAS NMR spectra of calcined mesoporous products (Figure S1), FTIR spectra in the OH stretching region after pyridine adsorption (Figure S2), and XRD patterns of samples before and after boiled in water for 120 h (Figure S3) (PDF). This material is available free of charge via the Internet at http://pubs.acs.org.

CM703676Y

(27) Kirschhock, C. E. A.; Buschmann, V.; Kremer, S.; Ravishankar, R.; Houssin, C. J. Y.; Mojet, B. L.; van Santen, R. A.; Grobet, P. J.; Jacobs, P. A.; Martens, J. A. *Angew. Chem., Int. Ed.* **2001**, *40*, 2637.